Vector-Diffraction Analysis of Finite Perfectly Conducting Gratings with Arbitrary Profiles

Fernando J. S. Moreira and Aluizio Prata, Jr.

Abstract

A vector diffraction formulation for the analysis of perfectly conducting gratings of finite width and thickness is presented. The grating is assumed to have a finite number of infinitely-long arbitrarily-shaped grooves, and is illuminated by an arbitrary plane wave. Electric and magnetic field integral equations are used to solve, exactly (in a numerical sense), the corresponding TM and TE electromagnetic problems. The capability of the formulation is demonstrated by analyzing and optimizing a grating-type polarizer with non-identical triangular grooves.

Keywords

Diffraction gratings, diffractive-optics devices, vector diffraction theory.

I. Introduction

Metallic gratings are widely used in optical applications (e.g., spectroscopy, filters, diffractive-optics devices, holography, etc.). They are also used at lower frequencies (microwave and millimeter-wave frequencies), primarily for wave polarization control. Currently available technologies permit the construction of metallic (or dielectric) gratings with extremely small features, suitable for high speed integrated optics operating at optical frequencies and beyond. Also, accurate blazes are now possible, permitting the construction of gratings with high diffraction efficiency operating at small wavelengths. When the grating features are sufficiently larger than the operational wavelength, scalar diffraction theory can be used to provide fast and accurate scattered field results [1]. However, when dealing with features comparable or smaller than the operation wavelength, one needs the more accurate modeling tools that can only be provided by vector diffraction theory [2].

Many authors have dealt with the analysis of optical metallic gratings using vector diffraction theory [2]. Generally they assume an infinite grating surface illuminated by plane wave. The scattered field is obtained applying Floquet's theorem (which accounts for the periodicity of the grating) and using two- (for unidirectional gratings) or three- (for bidirectional gratings) dimensional field integral equations, which are numerically solved using standard techniques [3],[4]. For the specific case of metallic gratings employing infinitely long rectangular grooves, it is also possible to determine the scattered field using parallel-plate waveguide modes to describe the field inside the grooves, and forcing the fields inside and outside the grooves to coincide at the grating surface [5],[6]. This technique can also be applied to other geometries for which a modal description of the fields inside the grooves can be obtained (e.g., [7]). It even can, at least in principle, handle gratings with arbitrary profiles, by approximating the grooves by small sections

Fernando J. S. Moreira is with the Department of Electronic Engineering of the Federal University of Minas Gerais, 30161-970 Belo Horizonte, MG, Brazil, fernando@eee.ufmg.br.

Aluizio Prata, Jr. is with the Department of Electrical Engineering–Electrophysics of the University of Southern California, Los Angeles, CA 90089-0271, USA, prata@hertz.usc.edu.

of parallel-plate waveguides and performing field matching at each junction. However, it is not numerically efficient in such cases. Gratings with a finite number of grooves have also been investigated, albeit less extensively [8]. As an example, Ref. [9] considers the case of a finite grating with infinitely long rectangular grooves, but the grooves are assumed located in an infinite perfectly conducting plane, and only one of the polarizations is treated. All these techniques can also handle arbitrary illumination (e.g., Gaussian beams), provided that the incident beam is represented by an angular spectrum of plane waves. As an example of this the reader is referred to [10], which treats the scattering of a two-dimensional Gaussian beam by a periodic infinite planar screen.

The objective of this work is to overcome some of the limitations of previous formulations, by presenting the numerical analysis of finite perfectly conducting gratings with arbitrary profiles, illuminated by an arbitrarily polarized plane wave, with its propagation direction also arbitrarily oriented. The fact that the incident plane wave can be completely arbitrary makes the formulation suitable for handling arbitrary illumination (e.g., three-dimensional Gaussian beams). In this work, the gratings are assumed to be made of a perfectly conducting material and to have a finite number of infinitely long grooves (features). Two-dimensional field integral equations are used to solve the scattering problem exactly (in a numerical sense). The grating surface may be curved along the direction perpendicular to the grooves, and hence concave gratings can be analyzed. For gratings that are finite on both directions (not treated here), three-dimensional field integral equations must be used, somewhat complicating the formulation [4].

This article has been divided in five sections. In Sect. II the two-dimensional electric and magnetic field integral equations, required to model the finite gratings of interest, are presented. This section also discusses the numerical solution of these equations using moment-method techniques with point matching [3]. Sect. III demonstrates the method presented in Sect. II by considering, as an example, a finite perfectly conducting grating with a triangular profile, operating as a polarizer. Its geometry has been chosen to reflect only the TM polarization (no magnetic field $\vec{H}$ along the groove direction) while totally backscattering the TE polarization (no electric field $\vec{E}$ along the groove direction), when an infinite number of grooves is used. Since the actual grating has a finite number of grooves, a numerical optimization procedure is incorporated in order to obtain the optimum finite-grating profile geometry (optimum in the sense of minimizing the reflection of the TE polarization). The article ends with an Appendix describing how to modify the theory presented for the case of an infinite grating.

II. Diffraction Grating Two-Dimensional Integral Equations

The geometry considered in this work is shown in Fig. 1, together with a convenient Cartesian coordinate system for its analysis. The grating is assumed to be made of a perfect conductor and has a finite number of arbitrarily-shaped infinitely-long grooves. The grating surface may be curved along the direction perpendicular to the grooves. The grooves can be different from each other and are not even required to have a constant period. An arbitrarily polarized plane wave, with an arbitrary propagation direction (given by the vector wavenumber $\vec{k}$), illuminates the grating as shown in Fig. 1. The objective here is the numerical determination of the vector electromagnetic fields scattered by such grating. The $\hat{z}$-direction is assumed parallel to the grooves—the grating geometry is independent of the z coordinate. These assumptions permit the present problem to be handled using a two-dimensional scattering formulation based on the electric and magnetic field integral equations (EFIE and MFIE, respectively) [4].

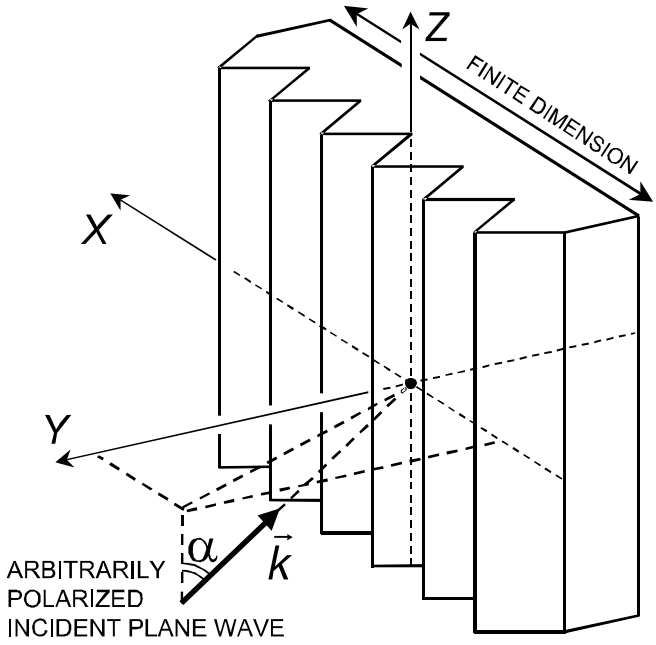

Fig. 1. Grating geometry.

Although the grating geometry does not depend on z, an oblique incident plane wave (i.e., $\alpha \neq 90°$) will introduce a z-dependence factor of the form $\exp(-jkz\cos\alpha)$ in the formulation, with $k = |\vec{k}| = 2\pi/\lambda$ (λ being the wavelength of the electromagnetic radiation). However, since this factor is common to all fields and currents, it is omitted in all subsequent equations. A time-harmonic dependence is assumed for the incident plane wave, and the corresponding factor $\exp(+j\omega t)$ (where $j = \sqrt{-1}$) has also been omitted in the present formulation.

The arbitrarily polarized incident plane wave can be conveniently decomposed into its corresponding TM and TE polarized counterparts (no magnetic $\vec{H}$ and electric $\vec{E}$ fields along the $\hat{z}$ direction, respectively), and each part can be handled separately. Since the total tangential electric field must be zero at the (perfectly conducting) grating surface, the EFIE of the TM polarization can be written as [4]:

$$E_z^{in}(\vec{\rho}) \; - \; \frac{\xi\eta\,\sin\alpha}{4}\int\limits_C H_0^{(2)}(\xi\,|\vec{\rho}-\vec{\rho}\,'|)\;\; J_z(\vec{\rho}\,')\;\; dl' \;\; = \;\; 0, \qquad (1)$$

where C is the grating cross-section contour (in the $z = 0$ plane), $E_z^{in}(\vec{\rho})$ is the $\hat{z}$-component of the incident electric field at an arbitrary point $\vec{\rho}$ located on the contour C, $J_z(\vec{\rho}\,')$ is the $\hat{z}$-component of the electric current density flowing at the point $\vec{\rho}\,'$ (also located at the contour C), $\xi = k\,\sin\alpha$, η is the free-space wave impedance ($\eta = 376.73031\,\Omega$), and $H_0^{(2)}$ is the zero-th order Hankel function of the second kind. For the TE polarization it is more convenient to use the MFIE, which is obtained by requiring the total magnetic field, immediately underneath the (perfectly conducting) grating surface, to be zero. This yields [4]:

$$H_z^{in}(\vec{\rho}) \; - \; \frac{H_z(\vec{\rho})}{2} \; - \; \frac{j\,\xi}{4}\int\limits_C \frac{(\vec{\rho}-\vec{\rho}\,')}{|\vec{\rho}-\vec{\rho}\,'|}\cdot\hat{n}\;\; H_1^{(2)}(\xi\,|\vec{\rho}-\vec{\rho}\,'|)\;\; H_z(\vec{\rho}\,')\;\; dl' \;\; = \;\; 0, \qquad (2)$$

where $H_z^{in}(\vec{\rho})$ is the $\hat{z}$-component of the incident magnetic field on the contour C, $H_z(\vec{\rho})$ is the $\hat{z}$-component of the total magnetic field (incident + scattered) immediately above the contour C, $\hat{n}$ is the outward pointing unit normal to the contour C, and $H_1^{(2)}$ is the first order Hankel function of the second kind. It is important to observe here that, since the MFIE is derived requiring the total magnetic field to be zero immediately underneath the grating surface, the MFIE can not be used for zero-thickness gratings (unless they are infinite).

The unknowns in (1) and (2) are the complex quantities J_z and H_z, which can be solved using the moment-method (MoM) technique. To accomplish this, J_z and H_z are expanded into a suitable set of basis functions over the integration contour C. In the present work sufficiently accurate solutions are obtained by applying the point matching procedure [3], which consists in approximating the contour C by small straight-line segments over which J_z and H_z are assumed constant, and enforcing (1) and (2) at the central point of each segment (testing points). This procedure transforms the EFIE (TM polarization) into the linear matrix equation

$$\left[E_z^{in}(P_m)\right] \;\; = \;\; \left[M_{mn}^{TM}\right] \;\; \left[J_z(P_n)\right], \qquad (3)$$

where

$$M_{mn}^{TM} \;\; = \;\; \frac{\xi\eta\,\sin\alpha}{4}\int\limits_{C_n} H_0^{(2)}(\xi\,|\vec{\rho}_m-\vec{\rho}_n|)\;\; dl_n, \qquad (4)$$

P_m and P_n are the central points of the $m-$th and $n-$th segments, respectively, $\vec{\rho}_m$ and $\vec{\rho}_n$ correspond to $\vec{\rho}$ and $\vec{\rho}\,'$ of the $m-$th and $n-$th segments, respectively, and C_n is the $n-$th segment of the contour C (see Fig. 2). For the MFIE (TE polarization) the corresponding integral equation is transformed into the linear matrix equation

$$\left[H_z^{in}(P_m)\right] \;\; = \;\; \left[M_{mn}^{TE}\right] \;\; \left[H_z(P_n)\right], \qquad (5)$$

where

$$M_{mn}^{TE} \;\; = \;\; \frac{j\,\xi}{4}\int\limits_{C_n} \frac{(\vec{\rho}_m-\vec{\rho}_n)}{|\vec{\rho}_m-\vec{\rho}_n|}\cdot\hat{n}_n\;\; H_1^{(2)}(\xi\,|\vec{\rho}_m-\vec{\rho}_n|)\;\; dl_n \;\; + \;\; \frac{\delta_{mn}}{2}, \qquad (6)$$

$\hat{n}_n$ is the outward unit normal to the $n-$th segment, and δ_{mn} is the Kronecker delta (unit if $m=n$ and zero if $m\neq n$). To obtain convenient closed-form expressions for (4) and (6) one assumes that each segment is sufficiently small (about 0.1 λ for smooth surfaces), so that the integrand value is approximately constant over them. This simplifies (4) and (6) to

$$M_{mn}^{TM} \;\; = \;\; \frac{\xi\eta\,\sin\alpha}{4}\Delta C_n\;\; H_0^{(2)}(\xi\,|\vec{\rho}_m-\vec{\rho}_n|), \quad \text{if} \;\; m\neq n, \qquad (7)$$

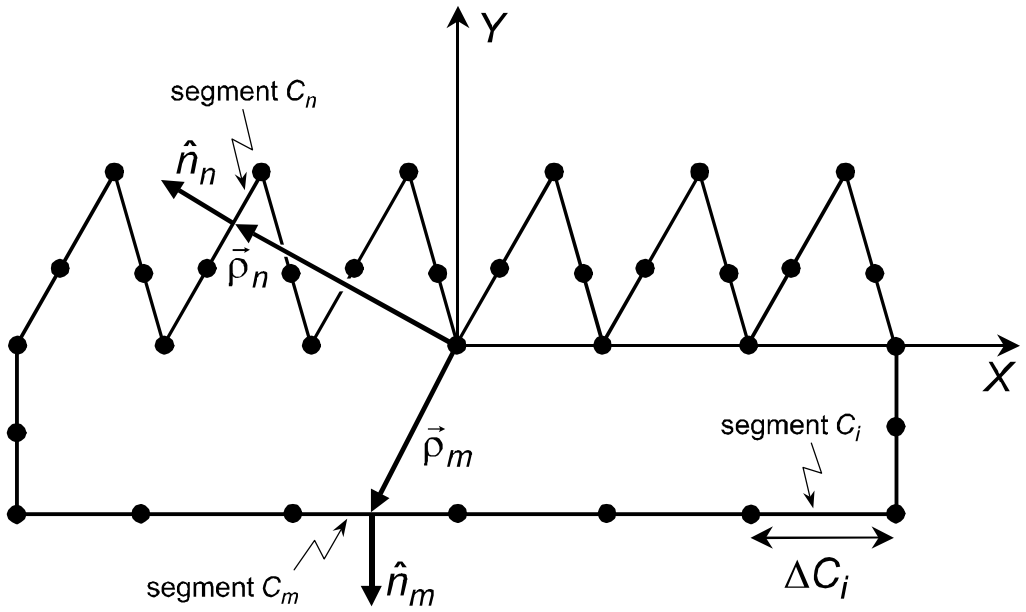

Fig. 2. Grating cross-section representation for the MoM solution.

$$M_{mn}^{TE} = \begin{cases} \frac{j\xi}{4}\Delta C_n \ \frac{(\vec{\rho}_m-\vec{\rho}_n)}{|\vec{\rho}_m-\vec{\rho}_n|}\cdot\hat{n}_n \ H_1^{(2)}(\xi\,|\vec{\rho}_m-\vec{\rho}_n|), & \text{if } m\neq n, \\ 1/2\,, & \text{if } m=n, \end{cases} \tag{8}$$

where ΔC_n is the length of the $n-$th segment and both $\vec{\rho}_m$ and $\vec{\rho}_n$ are now fixed at the central points of the $m-$th and $n-$th segments, respectively (see Fig. 2). When $m=n$, a convenient expression for M_{mn}^{TM} can be obtained by substituting the small argument approximation of the Hankel function into (4). This yields

$$\begin{aligned} M_{mn}^{TM} &= \eta\Delta\,\sin\alpha\left\{1-\frac{\Delta^2}{3}\left(1+\frac{2j}{\pi}\right)-\frac{2j}{\pi}\left[\ln\left(\Delta\,\exp(\gamma)\right)-1\right]\right. \\ &+ \left. j\frac{2\Delta^2}{3}\left[\ln\left(\Delta\,\exp(\gamma)\right)-\frac{1}{3}\right]\right\}, \quad \text{if } m=n, \end{aligned} \tag{9}$$

where $\Delta=\Delta C_n\ \xi/4$ and γ is the Euler's constant ($\gamma=0.57721...$). For grating cross sections approximated by N_S segments, each of the matrices $[M_{mn}^{TM,TE}]$ have $N_S\times N_S$ elements. However, by taking advantage of symmetries that may be present, unnecessary calculations can be avoided when evaluating these elements and/or solving the corresponding matrix equations [11]. However, in the examples presented below, none of such symmetries are present.

Once (3) and (5) are solved for the J_z and H_z, the scattered fields, produced at any distance from the grating, can be obtained using [11]

$$E_z^S(\vec{\rho}) = \frac{-\xi\eta\,\sin\alpha}{4}\ \sum_{n=1}^{N_S}\left[\ J_z(P_n)\ \int\limits_{C_n} H_0^{(2)}(\xi\,|\vec{\rho}-\vec{\rho}_n|)\ dl_n\ \right], \tag{10}$$

for the TM polarization, and

$$H_z^S(\vec{r}) \;=\; \frac{-\,j\,\xi}{4}\;\sum_{n=1}^{N_S}\left[\;\hat{\rho}\cdot\hat{n}_n\;\;H_z(P_n)\;\int\limits_{C_n} H_1^{(2)}(\xi\,|\vec{\rho}-\vec{\rho}_n|)\;\;dl_n\;\right], \tag{11}$$

for the TE polarization. For observation points located at distances much larger than the grating cross-section dimensions (herein called far-zone region), the above equations yield

$$\begin{aligned} E_z^S(\vec{\rho}) &= \frac{-\,\xi\eta\,\sin\alpha}{4}\sqrt{\frac{2}{\pi}}\;\exp(j\pi/4)\;\frac{\exp(-j\xi\rho)}{\sqrt{\xi\rho}} \\ &\times \sum_{n=1}^{N_S}\{J_z(P_n)\;\Delta C_n\;\exp[j\xi\,(x_n\,\cos\phi\,+\,y_n\,\sin\phi)]\}\,, \qquad (12)\\ E_\rho^S(\vec{\rho}) &= -\,\tan\alpha\;\;E_z^S(\vec{\rho}), \qquad (13)\\ H_\phi^S(\vec{\rho}) &= \frac{-1}{\eta\,\sin\alpha}\;E_z^S(\vec{\rho}), \qquad (14)\\ E_\phi^S(\vec{\rho}) &= H_\rho^S(\vec{\rho}) \;=\; H_z^S(\vec{\rho}) \;=\; 0, \qquad (15) \end{aligned}$$

for the TM polarization and

$$\begin{aligned} H_z^S(\vec{\rho}) &= \frac{\xi}{4}\sqrt{\frac{2}{\pi}}\;\exp(j\pi/4)\;\frac{\exp(-j\xi\rho)}{\sqrt{\xi\rho}} \\ &\times \sum_{n=1}^{N_S}\{\hat{\rho}\cdot\hat{n}_n\;H_z(P_n)\;\Delta C_n\;\exp[j\xi\,(x_n\,\cos\phi\,+\,y_n\,\sin\phi)]\}\,, \qquad (16)\\ H_\rho^S(\vec{\rho}) &= -\,\tan\alpha\;\;H_z^S(\vec{\rho}), \qquad (17)\\ E_\phi^S(\vec{\rho}) &= \frac{\eta}{\sin\alpha}\;H_z^S(\vec{\rho}), \qquad (18)\\ E_\rho^S(\vec{\rho}) &= E_z^S(\vec{\rho}) \;=\; H_\phi^S(\vec{\rho}) \;=\; 0, \qquad (19) \end{aligned}$$

for the TE polarization. In these equations the observation point is described by the polar coordinates ρ and ϕ, and x_n,y_n are the Cartesian coordinates of the $n-$th segment central point P_n. Note that (12)–(19) are only valid in the far-zone. Considerably different expressions result for the near-zone (for instance, the only components equal to zero in the near-zone are H_z^S and E_z^S, for the TM and TE polarizations, respectively).

For the TM polarization it is straightforward to show from (12)–(15) that the scattered power density is given by:

$$S^{TM}(\vec{\rho}) \;=\; \frac{1}{2\eta}\,|\vec{E}^S|^2 \;=\; \frac{1}{2\eta}\,\frac{|E_z^S(\vec{\rho})|^2}{\sin^2\alpha}. \tag{20}$$

In the same way [from (16)–(19)], for the TE polarization the scattered power density is given by:

$$S^{TE}(\vec{\rho}) \;=\; \frac{\eta}{2}\,|\vec{H}^S|^2 \;=\; \frac{\eta}{2}\,\frac{|H_z^S(\vec{\rho})|^2}{\sin^2\alpha}, \tag{21}$$

Throughout this work a plane wave with a 1 Volt/m electric-field amplitude has always been used to illuminate the gratings. Also, all scattered power density plots depict normalized values Σ given by

$$\Sigma \;=\; S \;\times\; \xi\rho. \tag{22}$$

The solution of (3) and (5) can become ill-behaved whenever the operation wavelength and angle of incidence of the impinging plane wave produce surface currents with z-dependence phase matching the one of a particular hollow cylindrical waveguide mode with wall coinciding with the grating cross section C. This difficulty is caused by the fact that the waveguide mode currents also satisfy the integral equations (1) and (2), while producing zero electromagnetic field outside the contour C. However, this problem can be eliminated by adding a few extra MoM testing points inside the grating cross section and forcing the total fields to be zero at these extra points [12]. This eliminates the surface current densities associated with the waveguide modes (since they always produce non-zero fields inside the contour C) while yielding an overdetermined system of equations, which can be solved by multiplying both sides of the corresponding matrix equation by the conjugate-transpose of the matrix—a procedure known as the Moore-Penrose pseudo-inverse method [12]. However, depending on the grating geometry, this matrix multiplication requires significantly more time than solving the final system of equations (even accounting for the time spent computing the initial matrix elements), and the computational efficiency of the scattering evaluations are reduced considerably. To avoid this drawback, the Moore-Penrose method should be employed only when necessary. This can be accomplished by using the near-zone (10) and (11) to find the scattered fields at a few selected points inside the grating cross section. When this and the incident plane-wave field are added, zero field should result. If this does not occur (within a certain tolerance, which in this work has been arbitrarily set to 10% of the magnitude of the incident electric field), a waveguide mode is considered to be present and only then the Moore-Penrose method is used.

The above formulation can be easily modified to handle the case of a perfectly conducting planar grating with an infinite number of identical periodic grooves illuminated by an arbitrarily plane wave, as demonstrated in the Appendix.

III. Numerical Examples

To illustrate the usage of the previously presented formulation, the determination of the electromagnetic field scattered by a metallic planar grating with a triangular profile is considered below. The geometry operates as a polarizer, reflecting only the TM polarization while totally backscattering the TE polarization [13]. The basic grating configuration is presented in Fig. 3. Initially the grating is assumed to have an infinite number of identical grooves, and the formulation of the Appendix is used to obtain J_z and H_z. To solve the field integral equations using the MoM technique, 10 segments are used in the smaller triangular side and 20 in the other ($N_S = 30$). Once J_z and H_z are determined, the grating is truncated to 1,000 grooves and (20) and (21) are used to obtain the scattered power density. The incident plane wavenumber vector $\vec{k}$ is parallel to the $z = 0$ plane ($\alpha = 90^\circ$) and makes an angle of 60° with the normal to the grating plane ($\beta = 330^\circ$ in the Appendix formulation). The operation wavelength is $\lambda = 1\,\mu$m, and hence the groove width is $0.57735\ \lambda$ (see Fig. 3). The normalized scattered power densities for both polarizations are shown at Fig. 4, from which we observe that basically only the TM polarization is reflected at $\phi = 30^\circ$, with a polarization isolation of about

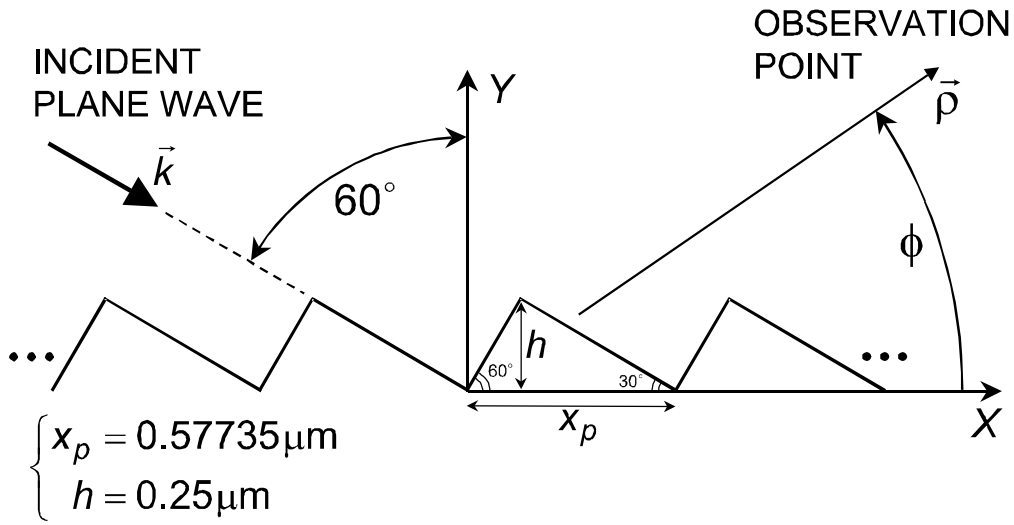

Fig. 3. Geometry of the infinite triangular grating.

50 dB. The diffraction efficiency of the grating can be calculated from the results shown in the figure, by determining the normalized scattered power density produced by a flat metallic plate with the same dimensions and illumination. In the present case, the corresponding flat plate scattered power density in the $\phi = 30°$ direction is 28.30 dB (for both polarizations). Hence, from Fig. 4 one can see that the diffraction efficiencies at $\phi = 30°$ are 90.2% (−0.45 dB) and 0.002% (−47.83 dB), for the TM and TE polarizations, respectively.

When the grating has a finite number of grooves the above behavior is expected to degrade somewhat, as the geometry has originally been designed to be infinite. To illustrate this, the analysis of a finite grating with 20 identical grooves is carried out with the formulation presented in Sect. II. The triangular groove geometry, plane-wave orientation, and wavelength are the same as before. In order to use the field integral equation formulation, for the TE polarization, the grating must have a finite thickness, as shown in Fig. 5. For the MoM analysis, once more 10 segments are used in the smaller triangular side and 20 in the other, for each one of the 20 grooves. 40 segments are used for each side wall and 360 segments for the wall located at $y = -1$ μm, yielding a total of $N_S = 1,040$ segments. The normalized scattered power densities obtained are shown in Fig. 6. The isolation between polarizations, at $\phi = 30°$ (reflection), has now degraded to approximately 37 dB. Also, since the total grating dimension is considerably smaller than the previous geometry, energy is removed from the peaks and scattered towards other regions, decreasing the polarization efficiency of the grating. The corresponding flat plate normalized scattered power density for this case, at $\phi = 30°$, is −5.56 dB and −5.47 dB for the TM and TE polarizations, respectively, which gives diffraction efficiencies of 90.2% (−0.45 dB) and 0.016% (−37.87 dB), respectively.

The next case study presents numerical optimization results for the coordinates of the 20-grooves-grating top triangular vertices, in an attempt to increase its polarization isolation, over the $\phi = 25°$ to 35° region. The grooves' width have been kept fixed at the previous value of 0.57735 μm. Again, the same incident plane wave is used to illuminate the grating. Only the coordinates of the first (1 in Fig. 5) and the last (20 in Fig. 5) top triangular vertices were optimized. With this the basic scattering characteristics of the

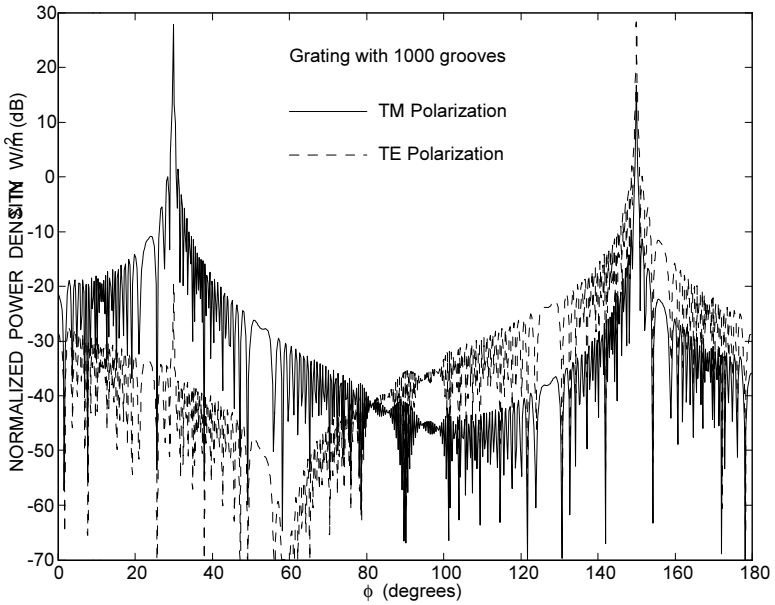

Fig. 4. Scattered power density of the infinite triangular grating.

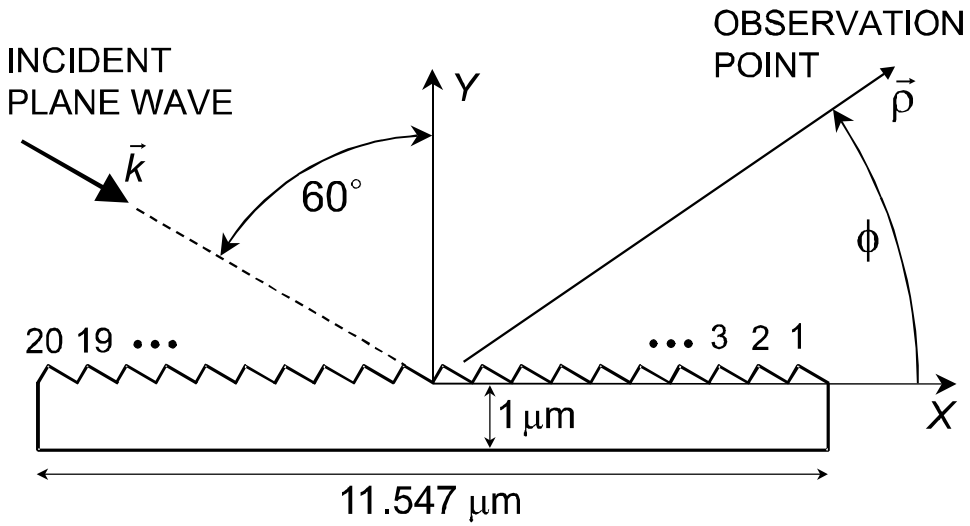

Fig. 5. Geometry of the finite triangular grating.

grating can be expected to remain the same and the optimization is only used to improve the polarization isolation in the desired region. The obtained Cartesian coordinates of the top vertices, $x_i + \delta x_i$ and $y_i + \delta y_i$ (with $i = 1$ and 20), are given in Table I. The coordinates x_i and y_i correspond to the non-optimized grating geometry of Fig. 5. The δx_i and δy_i are the required changes in the coordinates of the top vertices—the result of the numerical optimization procedure. These coordinate increments have not been allowed to vary by more than $\pm 0.25\,\mu$m, in order to maintain the basic triangular profile. The normalized scattered power densities of the initial and optimized gratings are given in Figs. 7a and 7b, for the TM and TE polarizations, respectively. As the figures show, for the TM polarization, the overall scattering behavior of the grating is maintained. There

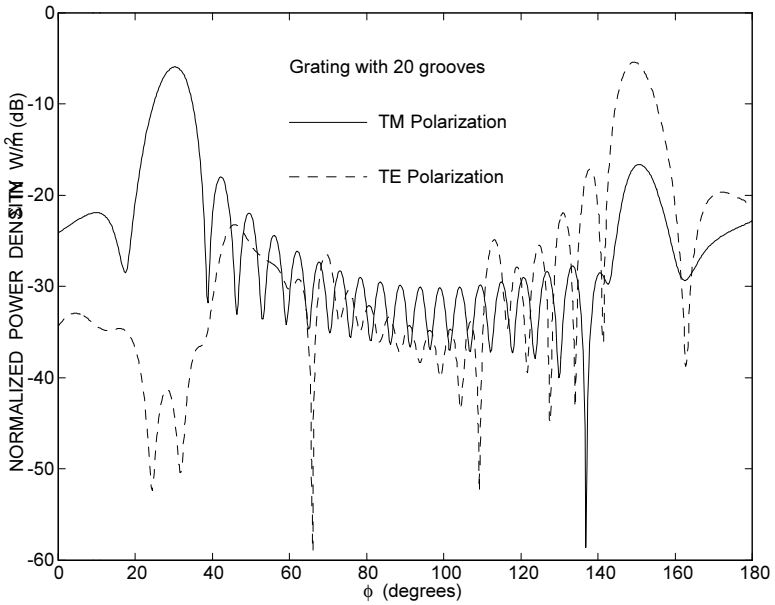

Fig. 6. Scattered power density of the finite triangular grating.

TABLE I
CARTESIAN COORDINATE INCREMENTS OF THE OPTIMIZED FINITE TRIANGULAR GRATING TOP VERTICES.

Groove	$\delta x_i(\mu\text{m})$	$\delta y_i(\mu\text{m})$
1	0.013	0.068
20	0.058	-0.021

is a $\sim$0.02 dB scattering decrease in the reflection direction ($\phi = 30°$), and a decrease of $\sim$0.4 dB in the backscattering direction ($\phi = 150°$). Also noticeable is an increase in the average power scattered in the $30° < \phi < 150°$ region. The optimization procedure improved the polarization isolation in the $25° < \phi < 35°$ by about 20 dB. The diffraction efficiencies of the optimized grating, at $\phi = 30°$, are 89.74% (-0.47 dB) and 0.0002% (-57.69 dB), for the TM and TE polarizations, respectively.

IV. CONCLUSIONS

The current development of optical components, and corresponding technology, permits the construction of gratings with accurate control of individual features. The reliable analysis and synthesis of such gratings are only possible using a rigorous vector diffraction theory, specially when all structural dimensions must be taken into account. A possible way to analyze these gratings is through the electric and magnetic field integral equations, which can be formulated for metallic and/or dielectric scattering surfaces. This technique has been explored in this article.

This work presented the two-dimensional electric and magnetic field integral equations required to exactly analyze the scattering of an arbitrarily polarized plane wave, with an arbitrary propagation direction, by a perfectly conducting grating with a finite number of

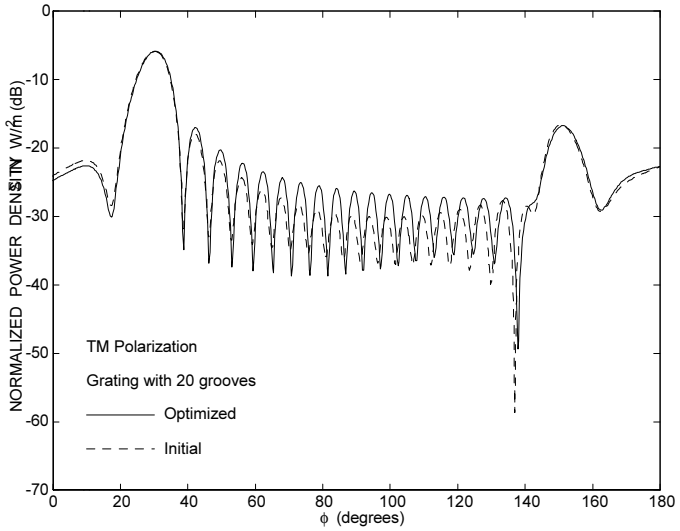

a) TM polarization.

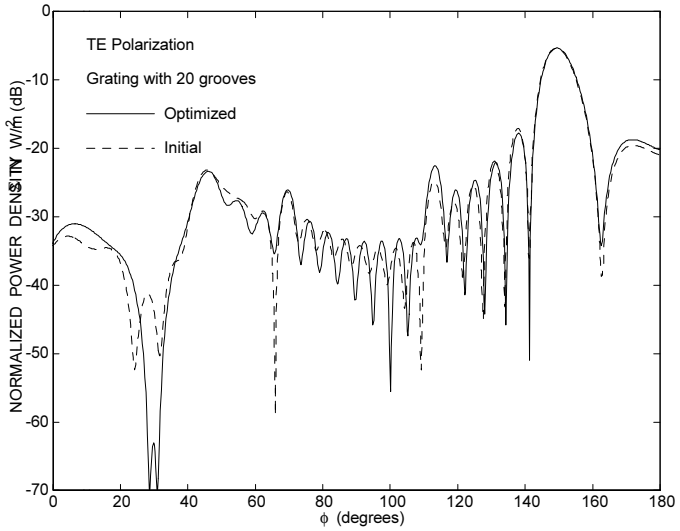

b) TE polarization.

Fig. 7. Scattered power density of the optimized finite triangular grating.

infinitely long grooves. The grating profile can be completely arbitrary along the direction perpendicular to the grooves.

As a test example of the formulation presented, the electromagnetic field scattered by a perfectly conducting planar grating with a triangular profile was investigated. The grating geometry was chosen such that it operates as a polarizer, reflecting only the TM polarization while totally backscattering the TE polarization. This grating was analyzed first assuming an infinite number of triangular grooves and then reducing its dimension to only 20 grooves. For the 20-groove geometry, the polarization isolation at the reflection direction decreased from ∼50 dB to ∼37 dB, basically because the groove geometry had been designed assuming an infinite number of grooves. To correct this the grating was numerically optimized, restoring the polarization isolation to a level of about 57.7 dB.

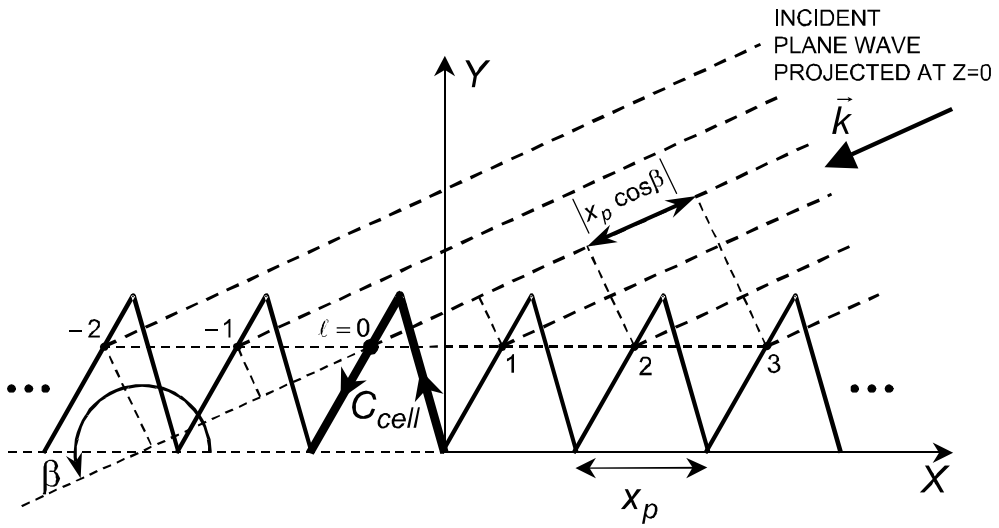

Fig. 8. Geometry of the infinite perfectly conducting planar grating.

These examples demonstrate the capability of the field integral equations for the accurate analysis and synthesis of finite-length gratings.

Appendix

Infinite Perfectly Conducting Planar Grating

When the planar grating has an infinite number of identical grooves, Floquet's theorem can be invoked to reduce the analysis task to just determining the scattering produced by a single groove. For a perfectly conducting grating, this corresponds to determining the induced current J_z and the field H_z (depending on the polarization of the illuminating plane wave) over only a single period [4]. Floquet's theorem is just the recognition that, for an infinite periodic geometry illuminated by a plane wave, the induced current J_z and the field H_z, at corresponding locations on any two different grooves, must have identical amplitudes and a phase difference identical to the one of the illuminating plane wave at the same locations (see Fig. 8). This property enables (1) and (2) to be rewritten as

$$E_z^{in}(\vec{\rho}) \; - \; \frac{\xi\eta \, \sin\alpha}{4} \sum_{\ell=-\infty}^{+\infty} \left\{ \exp(-j \, \ell \, \xi \, X_p \, \cos\beta) \int\limits_{C_{cell}} H_0^{(2)}(\xi \, |\vec{R}_\ell|) \;\; J_z(\vec{\rho}\,') \;\; dl' \right\} \;\; = \;\; 0, \tag{23}$$

$$H_z^{in}(\vec{\rho}) - \frac{H_z(\vec{\rho})}{2} - \frac{j\,\xi}{4} \sum_{\ell=-\infty}^{+\infty} \left\{ \exp(-j \, \ell \, \xi \, X_p \, \cos\beta) \int\limits_{C_{cell}} \frac{\vec{R}_\ell}{|\vec{R}_\ell|} \cdot \hat{n} \;\; H_1^{(2)}(\xi \, |\vec{R}_\ell|) \;\; H_z(\vec{\rho}\,') \;\; dl' \right\} \;\; = \;\; 0, \tag{24}$$

where

$$\vec{R}_\ell \;\; = \;\; \vec{\rho} - \vec{\rho}\,' - \ell \; X_p \; \hat{x} \tag{25}$$

and the other geometrical parameters are shown at Fig. 8. The integrations of Eqs. 23 and 24 are now evaluated over a single period (C_{cell}). However, an infinite summation appears in the above formulation, which is generally slowly convergent (and even divergent in many cases). References [14] and [15] present specific methods to efficiently evaluate the above series, when it is convergent.

Similarly to the finite grating geometry, Eqs. 23 and 24 can be solved using MoM techniques, as explained on Sect. II. Now, each entry of the $[M_{mn}^{TM,TE}]$ matrices will require the summation of a series, increasing considerably the computation time for each matrix entry. However, as the integration must be evaluated over only a single period, the number of matrix entries is reduced enormously.

It is important to observe that, once J_z and H_z are obtained, the scattered fields must then be determined. However, since the grating is now infinite on both directions, the approximations yielding (12)–(19) are no longer valid (the observation point is never in the grating far-zone region) and hence they can not be used. One then has to resort to perform a plane-wave expansion of the scattered field to determine the diffraction efficiency of the various diffraction orders. A way to avoid this difficulty is to use J_z and H_z of the infinite grating over a truncated grating. This allows (12)–(19) to calculate the scattered fields. If the grating has a large number of periods and its total dimension is much larger than the wavelength, this approximation yields very accurate results.

References

[1] M. Born and E. Wolf, *Principles of Optics*, 6th ed. (Pergamon, London, 1980).

[2] R. Petit (editor), *Electromagnetic Theory of Gratings*, (Springer-Verlag, Berlin, 1980).

[3] R. F. Harrington, *Field Computation by Moment Methods*, (IEEE Press, New York, 1993).

[4] R. Mittra (editor), *Computer Techniques for Electromagnetics*, (Taylor & Francis, Bristol, 1987).

[5] A. Wirgin and R. Deleuil,"Theoretical and experimental investigation of a new type of blazed grating," J. Opt. Soc. Am. **59**, 1348–1357 (1969).

[6] Y. L. Kok and N. C. Gallagher, "Relative phases of electromagnetic waves diffracted by a perfectly conducting rectangular-grooved grating," J. Opt. Soc. Am. A **5**, 65–73 (1988).

[7] S. Jovićević and S. Sesnic, "Diffraction of a parallel- and perpendicular-polarized wave from an echelette grating," J. Opt. Soc. Am. A **62**, 865–877 (1972).

[8] P. Facq, "Diffraction par des structures cylindriques périodiques limitées," Annales des Télécommunications **31**, 99–107 (1976).

[9] T. J. Park, H. J. Eom, and K. Yoshitomi, "Analysis of TM scattering from finite rectangular grooves in a conducting plane," J. Opt. Soc. Am. A **10**, 905–911 (1993).

[10] E. E. Kriezis, P. K. Pandelakis, and A. G. Papagiannakis, "Diffraction of a Gaussian beam from a periodic planar screen," J. Opt. Soc. Am. A **11**, 630–636 (1994).

[11] F. J. S. Moreira and Aluizio Prata, Jr., "Optimum strut cross sections for reflector antenna applications," Technical Report, Dept. Elect. Engineering, University of Southern California (1993).

[12] W. V. T. Rusch, J. Appel-Hansen, C. A. Klein, and R. Mittra, "Forward scattering from square cylinders in the resonance region with application to aperture blockage," IEEE Trans. Antennas and Propagat. **AP-24**, 182–189 (1976).

[13] E. V. Jull and J. W. Heath, "Reflection grating polarizers," IEEE Trans. Antennas and Propagat. **AP-28**, 586–588 (1980).

[14] R. Lampe, P. Klock, and P. Mayes, "Integral transforms useful for the accelerated summation of periodic, free-space Green's functions," IEEE Trans. Microwave Theory Tech. **MTT-33**, 734–736 (1985).

[15] R. E. Jorgenson and R. Mittra, "Efficient calculation of the free-space periodic Green's function," IEEE Trans. Antennas and Propagat. **38**, 633–642 (1990).